ELSEVIER

Journal of Alloys and Compounds 229 (1995) 144–157

Journal of ALLOYS AND COMPOUNDS

Chalcogenide misfit layer compounds

J. Rouxel[a], A. Meerschaut[a], G.A. Wiegers[b]

[a]*Institut des Matériaux de Nantes, UMR CNRS 110, Université de Nantes, 2, rue de la Houssinière, 44072 Nantes Cedex 03, France*
[b]*Chemical Physics, Materials Science Centre of the University, Nijenborg 4, 9747 AG Groningen, Netherlands*

Received 1 February 1995; in final form 8 March 1995

Abstract

Misfit layer chalcogenides $(MX)_{1+x}(TX_2)_m$ (M ≡ Sn, Pb, Sb, Bi, rare earth; T ≡ Ti, V, Cr, Nb, Ta; X ≡ S, Se; $0.08 < x < 0.28$; $m = 1, 2, 3$) result from an alternate stacking of MX and TX_2 slabs. Both sublattices have two *a* and *b* in-plane parameters; the ratio of the *a* parameters is irrational. The structural features associated with these planar intergrowth compounds are described. Multilayered misfit compounds ($m = 2, 3$) show various polytypes. Non-stoichiometry can occur in MX layers related to vacancies of M atoms (MX sublattice). The physical properties are discussed in detail. Superconductivity is observed in some series and can be studied as a function of *m*, the number of superconducting TX_2 slabs, such as $NbSe_2$, that can stack one on top of the other. In addition to interesting magnetic properties, transport measurements allow us to reach a better understanding of the electronic structure of the phases which appear, in many cases, as an infinite two-dimensional intercalation of MX slabs between TX_2 slabs with electron exchange between them. This leads to the introduction of a critical discussion of chemical bonds.

Keywords: Chalcogenides; Misfit phases; Transport properties; Superconductivity; Magnetic properties

1. Introduction

Misfit layer compounds have a composite (intergrowth) structure, made up of two or more interpenetrating sublattices (of different chemical composition) each with its own unit cell and space group [1,2]. Two types of composite compound exist, namely columnar or linear intergrowth compounds and planar intergrowth compounds.

A columnar composite crystal is made up of separate columns of different structural elements, or columns included in tunnels provided by another sublattice. Incommensurability comes from different periods along the direction of the columns/tunnels. Numerous examples are known of compounds with organic constituents. Inorganic examples include the $Ba_xFe_2S_4$ family ($0.062 < x \leq 0.143$) [3], the Sr_xTiS_3 phases [4] and the more complicated $A_{1-p}Cr_2X_{4-p}$ series (A ≡ Ba, Sr, Eu, Pb; X ≡ S, Se; $p \approx 0.3$) studied by Brouwer and Jellinek [5]. Fig. 1 shows the columnar structural type of $Ba_xFe_2S_4$ with an alternation of rows of barium ions and tetrahedral $[FeS_{4/2}]_1^\infty$ chains (edge-sharing FeS_4 tetrahedra). Fig. 2 shows the fascinating structure of $Eu_{1-p}Cr_2Se_{4-p}$ in which a framework with a composition $Cr_{21}Se_{36}$ provides two types of channel, parallel to each other, with either a sixfold or a threefold axis at the centre: $Eu_6Cr_2Se_6$ and Eu_3Se columnar sublattices are accommodated by the first and second types of channel respectively. In this case, there are three subsystems, namely the $Cr_{21}Se_{36}$ framework and the channels $Eu_6Cr_2Se_6$ and Eu_3Se. Along the channels the periodicity is different for the three subsystems.

When the channel axes are called the *a* axes, the general relation between the axes of the subsystems is given by the observation, from single crystal X-ray diffraction studies, that there is a common (*b**,*c**) plane in reciprocal space, which in real space means that not only are the *a* axes parallel and of incommensurate length ratio, but also their (*a*,*b*) planes and (*a*,*c*) planes are parallel. Therefore corresponding *b* and *c* axes do not need to be parallel, but have a length relation $b_1 \sin \beta_1 = b_2 \sin \beta_2$ and $c_1 \sin \gamma_1 = c_2 \sin \gamma_2$ (in the case of a compound with two subsystems, 1 and 2 refer to subsystems 1 and 2). Because of the common (*b**,*c**) plane, there is a common projection along the *a* axes. The general relationship between the axes of the composite crystal

SSDI 0925-8388(95)01680-5

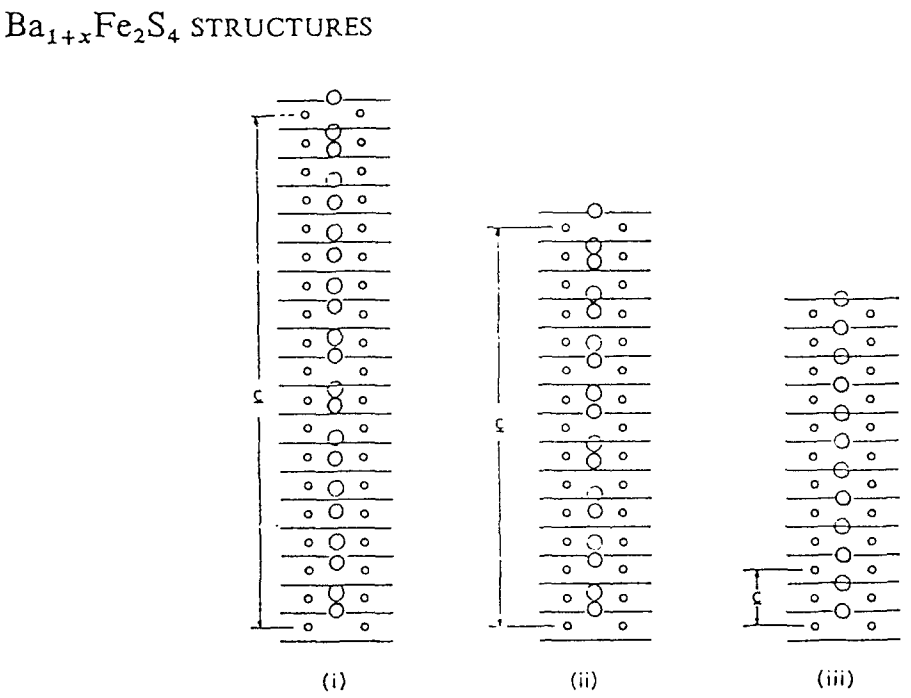

Fig. 1. Idealized representation of structures in the $Ba_{1+x}Fe_2S_4$ system showing (00*l*) layers of S atoms as black lines. The small circles represent Fe atoms and the large circles Ba atoms. (i) Structure of $Ba_5Fe_9S_{18}$. (ii) Proposed structure for $Ba_4Fe_7S_{14}$. (iii) Proposed structure for stoichiometric $BaFe_2S_4$. (After Ref. [3].)

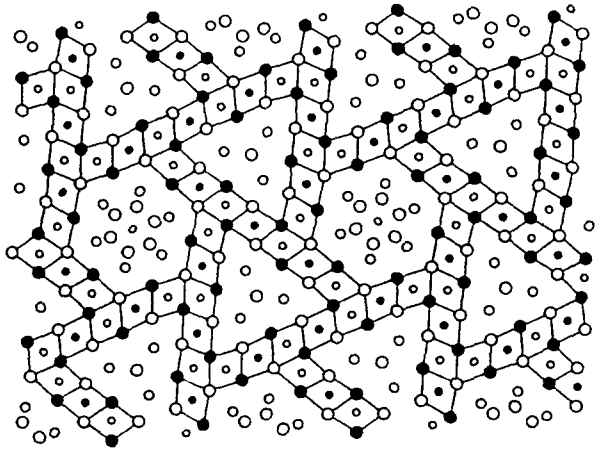

Fig. 2. The structure of $Eu_{1-p}Cr_2Se_{4-p}$ projected along the incommensurate axis. Large circles denote Se atoms, small circles represent Cr atoms and medium sized circles are Eu atoms. (After Ref. [5].)

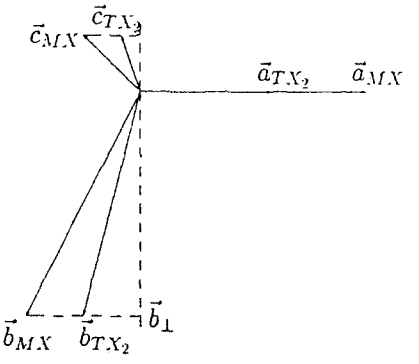

Fig. 3. The axes of the two subsystems MX and TX_2.

with two subsystems is shown in Fig. 3; for convenience, their origin is chosen to be the same.

The planar intergrowth compounds are made up of slabs; the parallel *a* axes (of incommensurate length ratio) form one of the in-plane axes of the two subsystems; again there is a common (b^*,c^*) plane in reciprocal space, and the [100] projection is common for the two subsystems. Misfit layer compounds are planar intergrowth compounds (see Fig. 4).

2. Misfit layer chalcogenides

2.1. General

Misfit layer chalcogenides $(MX)_{1+x}(TX_2)_m$ (with M ≡ Sn, Pb, Sb, Bi, rare earth; T ≡ Ti, V, Cr, Nb, Ta; X ≡ S, Se; $0.08 < x < 0.28$; $m = 1, 2, 3$) have a planar composite structure, composed of two layered subsystems, namely MX and $(TX_2)_m$ [6]. Layers of the two subsystems are stacked alternately one upon another. One of the in-plane axes of one subsystem (chosen to be the *a* axis) is parallel to the *a* axis of the second subsystem, the length ratio being incommensurate, and there is a common (b^*,c^*) plane. The MX slab has a

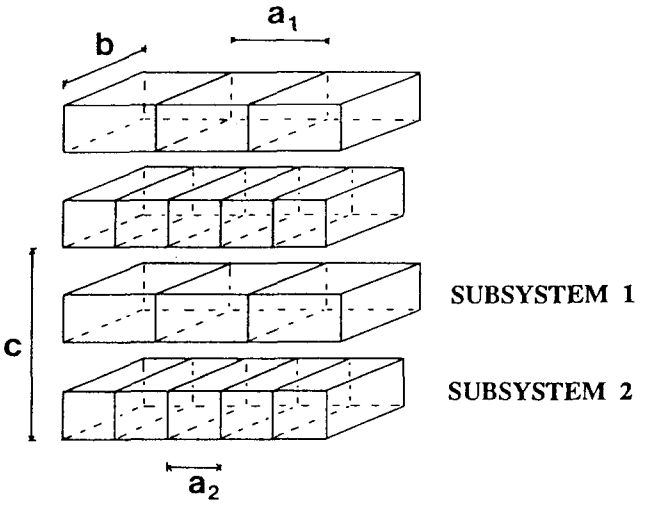

Fig. 4. Schematic representation of a planar composite structure.

pseudo-tetragonal symmetry; it consists of a two-atom-thick {001} slice of a rock-salt-like structure. The TX_2 sandwich is a three-atom-thick sandwich in which the transition metal T is surrounded by chalcogen atoms, either in octahedral coordination (T ≡ Ti, V, Cr) or in trigonal prismatic coordination (T ≡ Nb, Ta). Paired ($m = 2$) and even tripled sandwiches of TX_2, acting as a single subsystem, may occur.

The composition of the crystal, i.e. the ratio of MX to $(TX_2)_m$, is determined by the ratio of the a axes of the two subsystems (a_1 for MX, a_2 for TX_2). This is expressed by a variable $x = (4/2)(a_2/a_1) - 1$; 4/2 stems from the number of formula units per slab (4 for MX, 2 for TX_2). The length ratio a_1/a_2 is found to vary between 1.56 and 1.85 (the extreme values characterize $(YS)_{1.28}CrS_2$ [7] and $(BiS)_{1.08}TaS_2$ [8] respectively). Table 1 summarizes the unit cell dimensions of some misfit compounds.

2.2. Synthesis

These compounds can be prepared by heating the elements or a mixture of binary compounds (e.g. $Ln_2S_3 + TS_2$) in evacuated quartz ampoules at temperatures ranging from about 850°C (Pb, Sn derivatives) to 1050°C (lanthanide derivatives). A slight excess of sulphur or selenium is used.

Another route is to synthesize first the corresponding ternary oxide, specifically when lanthanide elements are involved. This oxide is then placed in a graphite boat and heated up to 1300–1350°C in flowing argon/H_2S gas. This sulphidizing process is generally complete after several hours. Such a technique was used for $(LaS)_{1.19}CrS_2$ starting from a mixture of $LaCrO_3$ and La_2O_3 in an appropriate ratio.

In order to obtain suitable crystals for single crystal X-ray investigations and physical measurements, vapour transport methods can be used. In some cases, iodine was added (less than 5 mg cm^{-3}); chlorine has also been used successfully (thermal decomposition of $(NH_4)_2PbCl_6$). Platelets with a black metallic lustre are obtained.

2.3. Crystal structure considerations

For most of the misfit layer compounds, the angles γ are equal to 90°. In this case, the b axes are parallel, and therefore $\vec{b}_1 = \vec{b}_2$. Exceptions are $(SbS)_{1.15}TiS_2$ and $(SbS)_{1.16}(TiS_2)_2$ for which the subsystem space groups are $C\bar{1}$ with $\alpha_1 = 83.97°$, $\beta_1 = 85.87°$ and $\gamma_1 = 84.06°$ for the SbS part and $\alpha_2 = 84.39°$, $\beta_2 = 82.82°$ and $\gamma_2 = 90.01°$ for the TiS_2 part, as reported for the $(SbS)_{1.15}TiS_2$ misfit compound [12].

For compounds with NbX_2 and TaX_2 subsystems (trigonal prismatic layer), it has been found that the α angle (between $\vec{b}$ and $\vec{c}$ axes) is equal to 90°. This is a consequence of the symmetry of a single TX_2 sandwich (mirror plane relating the X atoms of both planes sandwiching T) (Fig. 5(a)). The c axes may diverge ($\beta_1 \neq \beta_2 \neq 90°$); examples are $(YS)_{1.23}NbS_2$ [13] and $(HoS)_{1.23}NbS_2$ [14].

On the other hand, in the case of "octahedral" TX_2 sandwiches (i.e. T ≡ Ti, V, Cr), rows of chalcogen are displaced by $1/6b$ (Fig. 5(b)). The resulting symmetry is monoclinic with an angle given by $\alpha - 90° = \cos(b/6c)$. Examples are $(PbS)_{1.18}TiS_2$ [11] and $(PbS)_{1.12}VS_2$ [15]. More complicated situations may occur as illustrated by the triclinic symmetry of $(LaS)_{1.20}CrS_2$ [16] and $(SnS)_{1.20}TiS_2$ [17], for which the c axes diverge ($\beta_1 \neq \beta_2 \neq 90°$).

Table 1
Unit cell dimensions of some misfit compounds

Compound	a_1 (Å)	a_2 (Å)	$x = 2a_2/a_1 - 1$	$b_1 = b_2$ (Å)	$c_1 = c_2$ (Å)	α (°)	Reference
$(SnS)_{1.17}NbS_2$	5.673	3.321	0.1708	5.751	11.761	90	[9]
$(LaS)_{1.14}NbS_2$	5.828	3.310	0.1359	5.797	$c_1 = 11.52$[a] $c_2 = 23.94$	90	[10]
$(PbS)_{1.18}TiS_2$	5.800	3.409	0.1755	5.881	11.76	95.28	[11]

[a] $c_2 = 2c_1$; the LaS part is C-centred while the NbS_2 part is F-centred.

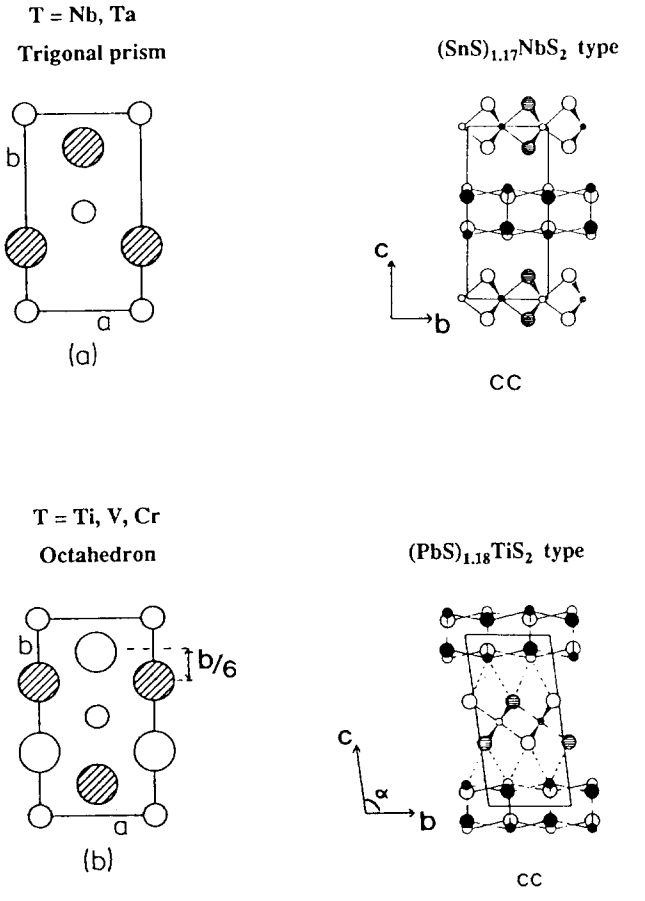

Fig. 5. Projection of the structure of a single slab of TX_2: (a) for the orthorhombic misfit compounds, with T in a trigonal prismatic coordination; (b) for the monoclinic misfit compounds, with T in a trigonal antiprismatic or distorted octahedral coordination. Large circles denote the S atoms, with open and hatched circles below and above the T atom plane respectively.

For all misfit layer compounds, the chalcogen atoms of both subsystems are found in rows parallel to [100]; rows in the same plane are $1/2\vec{b}$ apart. When looking at the complete structures as projected along [100], a common feature of all types of misfit layer compound is that M atoms are in between rows of sulphur parallel to [100] of the TX_2 lattice, making possible a bonding interaction of M with X of TX_2. There are two such rows in a unit cell, which leaves the possibility of two stacking sequences for each subsystem: a C-centred or an F-centred lattice. $(SnS)_{1.17}NbS_2$ is an example of a C-centred arrangement for both subsystems; the $\vec{c}$ axes are coincident. For the F-centred arrangement, there is an additional shift of $1/2\vec{c}$ which then gives a double $\vec{c}$ axis for the F-centred unit cell. According to this principle, four types of structure are possible, namely CC ($c_1 = c_2 \simeq 11$–12 Å), CF ($c_2 = 2c_1$), FC ($c_1 = 2c_2$) and FF ($c_1 = c_2 \simeq 22$–24 Å); the first letter refers to MX, the second to TX_2 (see Fig. 6).

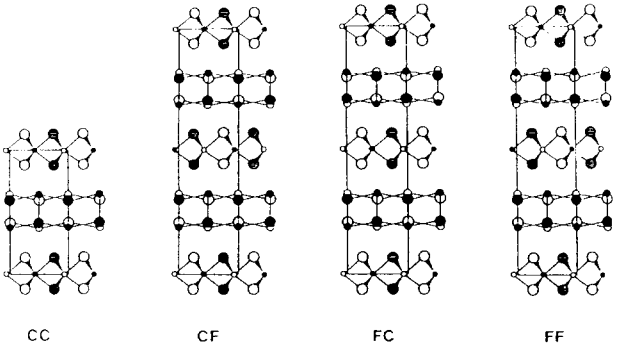

Fig. 6. Projections along [100] of misfit layer compounds with NbS_2 or TaS_2 sandwiches: CC type, CF type, FC type and FF type.

2.4. Description in superspace

The diffraction pattern of each of the two subsystems is given by a scattering vector $S = Ha^* + Kb^* + Lc^*$ in which a^*, b^* and c^* are the reciprocal lattice vectors. Because of the common b^*, c^* reciprocal vectors and the non-coincidence of the a^* axes, the diffraction pattern of both subsystems is given by four vectors, namely $S = Ha_1^* + Ka_2^* + La_3^* + Ma_4^*$ in which $a_1^* = a_{TX2}^*$, $a_2^* = b_{TX2}^* = b_{MX}^*$, $a_3^* = c_{TX2}^* = c_{MX}^*$ and $a_4^* = a_{MX}^*$. Reflections are therefore characterized by four integer indices $HKLM$. The $0KL0$ reflections are common to both subsystems; $HKL0$ reflections with $H \neq 0$ and $0KLM$ reflections with $M \neq 0$ are the TX_2 subsystem and the MX subsystem respectively. Reflections $HKLM$ of the composite crystal are satellites due to the mutual modulation of the two subsystems, the wave vector of the modulation of the TX_2 subsystem being a_4^* and that of the MX subsystem being a_1^*. Such satellite reflections were indeed observed by X-ray and electron diffraction. Janner and Janssen [18] were the first to note that a composite crystal can be described with superspace symmetry. A theory was developed, based on the theory for incommensurately modulated crystals; later extensions of this theory were made by van Smaalen [19], Yamamoto [20] and Kato and Onoda [21]. For the real structure, the three-dimensional (3D) space groups of the average structures of the subsystems are replaced by the (3 + 1)D superspace groups of their modulated structures. These subsystem symmetries can be derived uniquely from a single superspace group characterizing the symmetry [19].

In a structural determination using a conventional program such as XTAL, we can determine and refine the coordinates of the two subsystems separately in their 3D space groups; reflections $0KL0$ must be excluded because their intensities are determined by both subsystems. The $0KL0$ reflections are used for the determination of the y and z coordinates of the

atoms of one subsystem with respect to the other. The mutual modulation is visible in the parameters of thermal motion. Satellite reflections *HKLM* cannot be dealt with in this way; their intensities are determined by the displacive modulation of both subsystems. Programs for the refinement of coordinates, temperature factors and modulation parameters for composite crystals using X-ray intensities have been developed by Kato [22], Petricek et al. [23] and Yamamoto [20] based on his program REMOS for incommensurately modulated crystals [24]. These programs are a great improvement compared with conventional programs. Up to now several crystal structures have been determined using these programs. For only a few structures, satellites were measured and taken into account in the refinement. The modulation is also present in the intensity of the main reflections which means that the modulation can also be determined without satellites, but with larger standard deviations in the modulation parameters. The effect of the modulation on the distances between the atoms is given in a so-called *t* plot [25]. It is found that the main change compared with the average structure is that short distances between metal M and X of TX_2 become larger, while large distances become smaller. Furthermore, it is found that the coordination of M and T by X is much less symmetric than in the average structures.

3. Physical properties

The lubricating properties due to weak interlayer bonding of the Sn and Pb derivatives [26] and their superconducting properties [27–29] were major points of interest in these compounds in the early stages of research. Weak interlayer bonding is also reflected in very easy cleavage of the crystals. Indeed, anisotropy is a characteristic of the physical properties of misfit layer compounds.

We may formally consider the misfit compounds as intercalates of transition metal dichalcogenides 2H-TX_2 (T ≡ Nb, Ta) and 1T-TX_2 (T ≡ Ti, V, Cr), the intercalated species being the double layers MX. Some of these pristine dichalcogenides, namely 1T-VS_2, 1T-CrS_2 and 1T-$CrSe_2$, do not exist in a stable state. The structures and properties of the transition metal dichalcogenides and their intercalates M_xTX_2 (M ≡ alkali metals, Ib metals, transition metals, post- transition metals; T ≡ Ti, V, Cr, Nb, Ta) have been the subject of a large number of studies [30]. The properties have been described successfully in a rigid band model, which means that the only change in the electronic structure of the host is a change in band filling due to electron donation from the intercalated species. Intercalates with TiX_2, NbX_2 or TaX_2 sandwiches are metallic, while Cr compounds are semiconductors (even the non-stoichiometric compounds). Vanadium compounds take an intermediate position; non-stoichiometric compounds, e.g. Na_xVS_2 ($0 < x < 1$) are metals, while $NaVS_2$ is a semiconductor. It is shown that the description of misfit layer compounds as intercalates is not only formal since, in particular, the electrical transport properties are similar to those of the intercalates M_xTX_2, which prompted the suggestion that the conduction is in the TX_2 layers only. Misfit layer compounds with TiX_2, NbX_2 or TaX_2 sandwiches show metallic conductivity, while compounds with VX_2 or CrX_2 sandwiches show semiconducting or insulating behaviour.

Studies of the magnetic properties have shown that the rare earth compounds exhibit two-dimensional magnetism, the interaction between double layers being very weak; antiferromagnetic ordering and metamagnetic transitions occur below 4 K. Interesting compounds are those with a magnetic double layer as well as a magnetic sandwich (CrX_2); only a few of this type of compound have been investigated. Raman spectra of powdered samples of $(SnS)_{1.17}NbS_2$ and $(PbS)_{1.18}TiS_2$ [31] and single crystals of $(SnS)_{1.17}NbS_2$, $(PbS)_{1.14}NbS_2$ and $(PbS)_{1.18}TiS_2$ [32] have shown a superposition of the intralayer vibrations of individual layers; shifts of the intralayer vibration modes of NbS_2 relative to those of 2H-NbS_2 were interpreted in terms of charge transfer.

The optical reflectivity vs. frequency curves of the metallic misfit compounds show a minimum due to the plasma resonance of the charge carriers [33–37]. The plasma frequency yields the charge carrier concentration if the effective mass is known. By assuming the effective mass to be equal to that of the host TX_2, carrier concentrations can be estimated.

Photoelectron spectroscopy is an important tool for determining the valence band structure and charge transfer from the MX slabs to the TX_2 layers. The valence band structure as obtained by X-ray photoelectron spectroscopy (XPS) and UPS is almost a superposition of those of the parent constituents. For the Sn and Pb compounds the core levels point to divalent Sn and Pb, while for the rare earth compounds the trivalent state of the Ln ions was clearly established [38–45].

3.1. Electrical transport properties

The electrical conductivity of compounds with NbX_2 and TaX_2 sandwiches is metallic with in-plane resistivities ρ_{ab}, measured on crystals using a four-contact method, of about 10^{-6} Ω m (see Table 2 for a number of selected compounds). The resistivities follow a Grüneisen law with a Debye temperature of about 200 K. The ratio of the effective mass of the charge carriers along the (incommensurate) [100] direction

Table 2
Electrical transport properties of misfit layer compounds $(MX)_{1+x}TX_2$ and $(MX)_{1+x}(TX_2)_2$

Compound	ρ_{ab} (10^{-6} Ω m)		R_H (10^{-9} m^3 C^{-1})		z (h T^{-1}) (4 K)	α μV K^{-1}) (300 K)	Reference
	300 K	4 K	300 K	4 K			
$(SnS)_{1.17}NbS_2$	0.8	0.1	0.5	0.8	0.87	−19	[9]
$(PbS)_{1.14}(NbS)_2)_2$	0.2	0.2	1.4	2.2	0.24		[58]
$(SnS)_{1.17}(NbS_2)_2$[a]	40	20	1.0	1.2	0.43	−5	[58]
$(PbS)_{1.14}NbS_2$	3.2	0.2	2.5	3.5	0.20	−13	[106]
$(PbS)_{1.14}(NbS)_2)_2$[a]	80	36	1.2	1.7	0.31	−37	[58]
$(PbS)_{1.13}TaS_2$	1.6	0.1	1.0	1.5	0.48	−18	[107]
$(BiS)_{1.08}TaS_2$	1.2	0.1	0.56	1.1	0.62	−18	[8]
$(BiSe)_{1.09}TaSe_2$	2.8	1.2	0.16	0.77	1.0	−18	[108]
$(SnS)_{1.17}(NbS_2)_2$	2.7	0.3	2.5	3.5	0.18		[58]
$(LaS)_{1.14}NbS_2$	3.0	1.5	0.55	0.68	0.10	+50	[109]
$(CeS)_{1.16}NbS_2$	8.5	3.8	1.8	2.1	0.03	+28	[110]
$(SmS)_{1.19}TaS_2$	21	5.0	1.2	1.4	0.05	+30	[55]
$(SnS)_{1.20}TiS_2$	0.5	5.0	−2.8	−3.5	0.26	−35	[57]
$(SnS)_{1.20}(TiS_2)_2$	3.0	35	−6.0	−7.8	0.08		[58]
$(PbS)_{1.18}TiS_2$	0.18	2.0	−1.0	−1.7	0.74	−30	[57]
$(PbS)_{1.18}TiS_2$[a]	11	20	−2.9	−3.4	0.26	−35	[58]
$(PBS)_{1.18}(TiS)_2)_2$[a]	1.1	2.7	−2.7	−3.0	0.20	−60	[58]

[a] Measurement on compacted powder.

and the (commensurate) [010] direction of $(PbS)_{1.13}TaS_2$, as determined from optical reflectivity, is close to unity [34]. Resistivity measurements along these directions in the case of $(CeS)_{1.16}NbS_2$ also show the resistivity ratio ρ_a/ρ_b to be close to unity [46]. The resistivity along $\vec{c}$, measured using a four-contact method, indicates an anisotropy ρ_c/ρ_{ab} of about 50 for some rare earth compounds [46], while the anisotropy for $(SnS)_{1.17}NbS_2$ is as large as 250 at 300 K and 800 at 4 K [47]. Measurements of ρ_c using a two-contact method, giving much higher ratios of 10^4–10^5, are probably erroneous due to contact resistances. The anisotropy can also be determined in the superconducting state (see below). Indeed, the anisotropy can be derived from the angular dependence of H_{c2} on θ (angle between H and the (a,b) plane): $\epsilon = H_{c2,\parallel}/H_{c2,\perp} = (m_\perp/m_\parallel)^{1/2}$; an anisotropy with $\epsilon^2 = m_\parallel^*/m_\perp^* = \rho_c/\rho_{ab} \approx 100$ was deduced [48–50].

For the Sn, Pb and Bi derivatives, a positive Hall coefficient (R_H) and negative Seebeck coefficient (α) are found, as in the case of the intercalates Ag_xNbS_2 [51] and Ag_xTaS_2 ($0 < x < 0.67$) [52]. R_H values, calculated by assuming that only holes contribute ($R_H = 1/pe$, where p is the number of holes per unit volume and e is the elemental charge), correspond to a d_{z^2} band which is now more than half-filled. An electron donation from MX to TX_2 has taken place as in silver intercalates. In Table 2, hole numbers (z) (the number of holes per TX_2 formula unit from R_H at 4 K) are given. The donation of electrons, from MX to TX_2, has also been followed by photoelectron spectroscopy [38–45]. On the basis of the rigid band model, we expect, in the case of electron donation from MX to

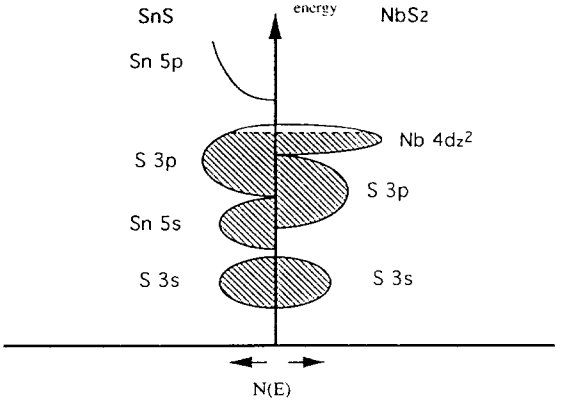

Fig. 7. Density of states vs. energy diagram of the two subsystems SnS and NbS_2 of $(SnS)_{1.17}NbS_2$. The band structure calculation showed that Sn 5s hybridized with S 3s, 3p is at the Fermi level.

TX_2, a decrease in the number of holes in the d_{z^2} band of T ≡ Nb and Ta and an equivalent number of holes in the valence band of MX (Fig. 7), and therefore a contribution to the conductivity from both types of hole. In the case that the mobilities are the same, R_H corresponds to one hole per Nb atom. In view of the presence of holes as well as electrons (negative α), the number of holes calculated using $R_H = 1/pe$ has only a qualitative meaning and definite conclusions about a contribution from the MX layers cannot be drawn. A band structure calculation by Fang et al. [53] of $(SnS)_{1.17}NbS_2$ in a commensurate approximation, i.e. with a ratio of the $\vec{a}$ axes of SnS and NbS_2 of 5/3 and therefore a theoretical composition $(SnS)_{1.20}NbS_2$, showed that there is a charge transfer from SnS to NbS_2 of about 0.4 electrons per Nb atom and that the

rigid band model does not work. It also showed that there is a strong mixing of the Sn 5s orbitals with 3p of S of NbS_2. Calculated and experimental XPS valence band spectra are compared in Fig. 8.

The rare earth misfit compounds with NbX_2 or TaX_2 sandwiches show a positive R_H, corresponding to about 0.1 hole per T atom in the d_{z^2} band. There is also a positive α, indicating that only holes contribute to the conduction. Optical reflectivity data [33–37] are also in agreement with a much lower carrier concentration compared with the Sn-, Pb- and Bi-based compounds. The intralayer Ln–X distances and photoelectron spectroscopy are in agreement with trivalent rare earth metals [42,43,45]. The hole numbers, about 0.1 holes per T atom, indicate an electron donation of 0.9 electrons per Nb or Ta (Table 2). This means that, when all Ln is Ln^{3+}, there must be electrons in an Ln 5d conduction band for a rigid band model (Fig. 9). A contribution of electrons in this conduction band to the electron conduction would therefore be expected; such a contribution is, however, not visible in the properties. It was therefore supposed by Suzuki et al.

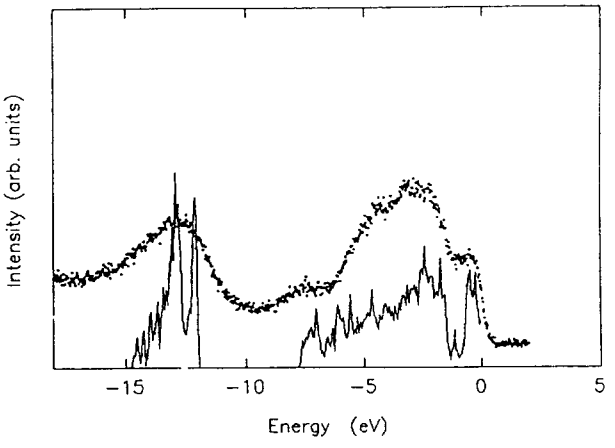

Fig. 8. XPS of the valence band of $(SnS)_{1.17}NbS_2$ (dots) compared with the calculated spectrum.

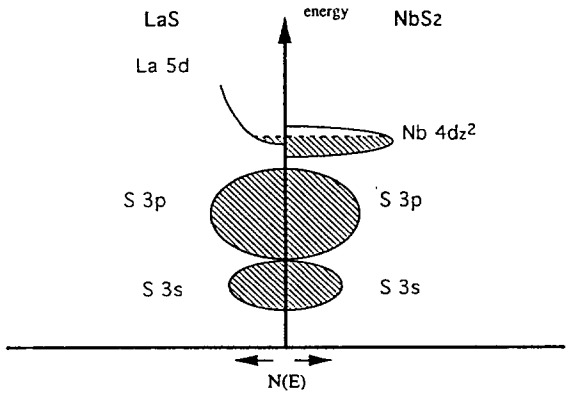

Fig. 9. Density of states vs. energy diagram of the two subsystems LaS and NbS_2 of $(LaS)_{1.14}NbS_2$.

[54] that the excess electrons on the LnX layer are localized. Such a localization was assumed to take place at the Ln sites owing to the varying lattice potential along [100] due to the mutual modulation of the two types of layer. On the basis of a particular example, another explanation is proposed below.

A thorough analysis of the transport properties of $(SmS)_{1.19}TaS_2$ was published recently by Suzuki et al. [45]. The resistivity vs. temperature behaviour was analysed using the Grüneisen equation for the acoustic phonon part; a Debye temperature θ_D of 250 K, close to that of $(LaS)_{1.14}NbS_2$ [49], was obtained. The Hall coefficient was found to be nearly temperature independent and corresponds to 0.052 holes per Ta atom (to compare with 0.05 holes per Ta atom measured by Wiegers et al. [55]). The magnetoresistance measured at 4 K with the field along the $\vec{c}$ axis is very small and suggests that the charge carriers are holes only. An analysis of the thermoelectric power in terms of a phonon drag term (in which electron–phonon and phonon–phonon interaction and domain boundary scattering were taken into account) and an electron diffusional part yielded a Fermi energy $E_F = 0.44 \pm 0.04$ eV. The analysis showed that domain boundary scattering is significant. They considered that the domain boundary scattering originates from the lattice incommensurability, which induces domain boundaries by forming discommensurations. Using $E_F = (h/2\pi)k_F^2/m^*$, with $m^* = 1.4m_o$, known for 2H-TaS_2, $k_F = 4.2 \times 10^9$ m^{-1}. Since $k_F v_s$ is known from the analysis of the thermopower, the sound velocity v_s can be estimated as 2.6×10^3 m s^{-1}. From this, the Debye temperature is calculated using $\theta_D = (h/2\pi)v_s(6\pi^2 N)/k_B T$; $\theta_D = 290$ K in reasonable agreement with $\theta_D = 250$ K from the resistivity measurements. It may be noted that there is no evidence for discommensurations from structure refinements, e.g. for $(LaS)_{1.14}NbS_2$ [25] and $(HoS)_{1.23}NbS_2$ [56], for which the mutual modulation was accurately determined.

Compounds with TiS_2 sandwiches and M ≡ Sn and Pb show metallic-type resistivity, where the temperature dependence of $\rho_{ab} = \rho_{ab}^o + AT^n$ with the exponent n equal to about 1.5 [57,58]. A similar temperature dependence has been noted for TiS_2 [59,60], Li_xTiS_2 [61] and Ag_xTiS_2 [62]; the exponent n is as high as 2.3 for TiS_2 and decreases with increasing silver content (when $x = 0.4$, $n \approx 1.5$) [62]. R_H and α are negative, as for silver intercalated TiS_2, and correspond to the partial filling of the broad conduction band of TiS_2 by transferred electrons. For compounds $(MS)_{1+x}(TS_2)_m$ with $m = 1$, the filling of the 3d band is 0.4–0.7 electrons per Ti atom while about half of these values are found for $m = 2$. In the same way as argued for the misfit compounds with NbS_2 or TaS_2 sandwiches, we expect, in addition to electrons in the 3d band of Ti, holes in the valence band of MS (Fig. 10, for a rigid

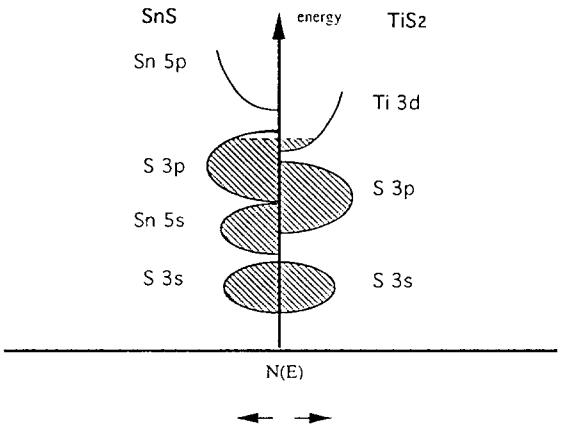

Fig. 10. Density of states vs. energy diagram of the two subsystems SnS and TiS_2 of $(SnS)_{1.20}TiS_2$.

band model); the Hall coefficient will be determined by the ratio of the mobilities of the electrons in the 3d band of the sandwiches and the holes in the valence band of the double layers. The properties do not show such a contribution. Moreover, the temperature dependence of ρ_{ab} suggests that the conduction is in the TiS_2 sandwiches only. This may mean that a rigid model does not work, or that holes in the MS valence band are localized, presumably on the M atoms due to the varying lattice potential along [100] creating sites favourable for localization. Defects in the MX layers may also be responsible, e.g. Ti^{3+} atoms substituted for M^{2+} [63], or vacancies in the chalcogen lattice of MX.

Compounds with VX_2 sandwiches show semiconducting properties. The distances between the V atoms in $(PbS)_{1.12}VS_2$ are 3.256 (2×) and 3.334 (4×) Å [15] and close to those of VS_2 (3.221 Å) which only exists in a metastable state [64]. Alkali metal intercalates, such as $LiVS_2$ with a V–V distance of 3.380 Å [65] and the non-stoichiometric compounds Na_xVS_2 ($0 < x \leq 1$) (V–V = 3.288 Å for $x = 0.3$; V–V = 3.346 Å for $x = 0.95$), are also metallic, while $NaVS_2$ is a semiconductor with V–V distances of 3.566 Å [66,67]. For $(PbS)_{1.12}VS_2$, an electron donation of about 0.3–0.6 e^- is estimated to take place from PbS to VS_2 layers (similar to that obtained for the TiS_2 compounds). Metallic-type conduction by electrons in the 3d conduction band of vanadium and by holes in the valence band of PbS is therefore expected. The observed semiconducting behaviour of this compound indicates that, in VS_2 sandwiches separated by a double MS layer, localization occurs for smaller V–V distances than in the 3D intercalates, and holes in the valence band of PbS do not contribute; they are localized or absent due to defects. Numerous studies have dealt with the electrical properties of $(LnS)_{1+x}VS_2$ phases [68,69]. Complex behaviour is observed which is not yet perfectly understood. For example, the resistivities of all samples increase gradually with decreasing temperature, although they do not show a simple activation mechanism. In Sm compounds, a semimetallic phase was prepared in addition to a semiconducting phase [68]. Cho et al. [70] found semiconducting behaviour of "$LnVS_3$" compounds (Ln ≡ La–Gd) from room temperature to 200 K. A semiconducting to metal transition has been reported at lower temperatures (150–200 K) for the La–Nd compounds. On the other hand, a recent study on $(LaS)_{1.19}VS_2$ single crystal (with V–V distances of 3.39 Å) confirms a semiconducting behaviour with an activation energy of 47 meV in the 300–150 K region that falls to 2.6 meV in the 4–30 K region (probably due to the presence of impurity levels) [71].

Compounds with CrS_2 sandwiches occur only in combination with rare earth metals. An optical gap of 1.2–1.3 eV was reported for compounds designated as $LnCrS_3$ (Ln ≡ Y, Gd, Dy, Ho and Er) by Takahashi et al. [72]. Chemical shifts of the K absorption edge and XPS binding energies of core levels in "$LnTS_3$" phases (Ln ≡ La, Nd and Gd; T ≡ V, Cr) indicate that the transition metal is trivalent [73]. The chromium compounds are semiconductors with an activation energy, deduced from resistivity data, in the range 0.48–0.56 eV. Resistivity measurements performed on a single crystal of $(GdS)_{1.27}CrS_2$ showed a semiconducting behaviour with an activation energy of 0.34 eV [74]. This semiconducting behaviour is at first rather surprising. Assuming that one electron has been transferred to the CrS_2 slab, reducing chromium to Cr^{3+} species, x electrons should remain in the LnS layer with respect to the $(LnS)_{1+x}CrS_2$ formulation. The Cr–Cr distances are too long to allow electron delocalization in the CrS_2 slabs. However, the remaining x electrons in the LnS slabs should be delocalized in a 5d band as in LaS, for example. A very precise chemical analysis (Cameca SX 50 electron microprobe) on a crystal of the "$GdCrS_3$" misfit compound was made. The exact chemical formula is $(Gd_{0.91}\square_{0.09}S)_{1.27}CrS_2$. Including the vacancies in the composition leads to an exact charge balance between Gd^{3+}, Cr^{3+} and S^{2-} ($0.91 \times 1.27 \times Gd^{3+} + Cr^{3+} = 6.48$; $3.27 \times S^{2-} = 6.54$) [74]. The electron transfer from the [GdS] to the [CrS_2] layer is such that no excess electrons exist. This is obviously a very important breakthrough that may help to understand other cases under discussion.

An accurate structural determination (including the modulation) by Ren et al. [75] showed that vacancies are also present on the La lattice of $(La_{0.95}Se)_{1.21}VSe_2$ such that charge balance exists between La^{3+}, V^{3+} and Se^{2-}. This compound sheds some light on the localization process in VSe_2 layers. Remarkably, the largest modulation amplitudes are at the vanadium atoms (not on La and Se of the double layer as noted for the rare

earth- and Sn-, Pb- and Bi- based compounds with NbS_2 or TaS_2 sandwiches). From the average V–V distances (3.58 (2×) and 3.54 (4×) Å), we expect, in comparison with VSe_2 (metallic, V–V = 3.356 Å [76]), $LiVSe_2$ (metallic, V–V = 3.53 Å [77]), $Na_{0.6}VSe_2$ (metallic, V–V = 3.43 Å) and $NaVSe_2$ (semiconducting, V–V = 3.75 Å [66,77]), a metallic-type conduction by electrons in the 3d band of V^{3+} ($3d^1$) [67,78]. The observed semiconducting behaviour again hints at stronger localization of the 3d electrons in single sandwiches compared with the 3D intercalates. The strong modulation amplitudes of the vanadium atoms indicate a modulation-induced localization (by the $La_{0.95}Se$ layers) of the 3d electrons of vanadium. Charge balance explains the lack of a contribution of the $[La_{0.95}Se]$ layers to the conductivity.

3.2. Magnetic properties

3.2.1. "$LnNbS_3$" compounds

Magnetic measurements on rare earth compounds with NbS_2 (or TaS_2) sandwiches [79–88] show that Ln is present as Ln^{3+}; exceptions are the samarium compounds, for which a contribution of Sm^{2+} was necessary to explain the properties [45]. The compound $(LaS)_{1.14}NbS_2$ shows only a small magnetic moment of La, indicating that La is predominantly La^{3+} [79,80]. A large crystal field effect is present for the Ce and Nd compounds with single or paired sandwiches [45,80,82,88]. The results indicate that the intralayer magnetic interaction is weakly ferromagnetic, while the interaction between LnS layers is even weaker, but antiferromagnetic. Indeed, below about 4 K, antiferromagnetic ordering occurs; the magnetic moments are oriented perpendicular to the layers. Metamagnetic transitions are observed in magnetization vs. field parallel to $\vec{c}$ measurements below 4 K.

For Gd compounds, a crystal field effect is not present due to the $^8S_{7/2}$ ground state of Gd^{3+}. The magnetic moment is close to that for free Gd^{3+} ions. Antiferromagnetic ordering occurs at 4.6 K for $(GdS)_{1.21}NbS_2$. The moments are in the layer, probably due to the large dipole–dipole interaction between Gd^{3+} ions [80]. The Tb and Dy compounds show almost Curie–Weiss behaviour with magnetic moments close to those for free Tb^{3+} and Dy^{3+} ions [6]; down to 4 K there are no signs of antiferromagnetic ordering. The absence of a crystal field effect may be ascribed to the contraction of the 4f orbitals from Ce to Tb and Dy.

3.2.2. "$LnVS_3$ compounds"

The magnetic properties of $(LnS)_{1+x}VS_2$ compounds with Ln ≡ La, Ce, Nd and Sm and VS_2 sandwiches are essentially determined by the LnS layers [68,69]. Again Ln is present as Ln^{3+}. The properties are largely similar to those of rare earth compounds with NbS_2 or TaS_2 sandwiches. A difference concerns the antiferromagnetic interaction between LnS layers which is stronger for the vanadium compounds.

For example, $CeS_{1.19}VS_2$ shows a Curie–Weiss behaviour above 100 K [68,69]; the effective magnetic moment is 2.84 μ_B. The deviation observed below 100 K from the Curie–Weiss law is explained by a crystal field effect. An antiferromagnetic transition is observed at 6.65 K; the Ce moments are oriented parallel to the $\vec{c}$ axis. A metamagnetic transition is visible in magnetization curves at 2 and 4 K with the field parallel to $\vec{c}$; at 2 K the transition occurs under 1 kOe.

3.2.3. "$LnCrS_3$ compounds"

Studies on misfit compounds with $[CrS_2]$ slabs at low temperatures show a complex behaviour associated with the Cr^{3+} layers. For example, $(LaS)_{1.20}CrS_2$ (presumably $(La_{0.95}\square_{0.05}S)_{1.20}CrS_2$ with La vacancies in the LaS lattice such that charge balance exists) exhibits a Curie–Weiss behaviour in the 110–300 K temperature range, with Cr^{3+} spin only contributions [86,87]. At about 120 and 70 K, two transitions are observed. $CuCrS_2$ [89,90] and $LiCrS_2$ [65], which show similar CrS_2 layers, may help to propose interpretations by taking into account the strength of the couplings with respect to the Cr–Cr distances and the type of ordering at low temperature. $CuCrS_2$ shows helical magnetic ordering below 39 K [91]. $LiCrS_2$ shows a 120° spin structure in the layers with antiferromagnetic ordering between the layers. A frustrated situation has been envisioned within the CrS_2 sandwiches in $(LaS)_{1+x}CrS_2$ followed, below 65 K, by either a spin glass behaviour or superparamagnetism [92]. Antiferromagnetic and helimagnetic transitions have also been proposed [87]. Neutron studies are now in progress to shed light on the low-temperature magnetic structures which express a complex competition between ferromagnetic and antiferromagnetic coupling in one Cr^{3+} layer as a function of the modulated Cr–Cr distances. In addition, the easy axis of magnetization may change from one compound to another. Measurements on $(NdS)_{1+x}CrS_2$ crystal show that $\vec{c}$ is the direction of easy magnetization [86]; in the gadolinium phase, it is in the (*a*,*b*) plane [93].

3.3. Superconductivity

Superconductivity in the layered transition metal dichalcogenides (2H-NbS_2, T_c = 6.3 K; 2H-TaS_2, T_c = 0.65 K; 2H-$NbSe_2$, T_c = 7.2 K; 2H-$TaSe_2$, T_c = 0.15 K) and the intercalates with organic molecules has aroused great interest in the past. The dichalcogenides are type II superconductors with a large anisotropy of the critical field ($H_{c2,\parallel} > H_{c2,\perp}$; $\parallel$ and $\perp$ denote *H*

parallel and perpendicular to the layers respectively), which is even more pronounced on intercalation with organic molecules. There is, however, no substantial increase in T_c on intercalation with organic molecules. Superconducting transitions are observed for compounds $(MX)_{1+x}(TX_2)_m$ (M ≡ Sn, Pb, Bi; X ≡ S, Se; $m = 1, 2$). The transition temperatures are below 4 K, except for $(PbSe)_{1.14}(NbSe_2)_3$ [94] and $(LaSe)_{1.14}(NbSe_2)_2$ [95] with $T_c = 4.8$ and 5.3 K respectively.

The superconducting transition of $(PbS)_{1.14}NbS_2$ [48] is shown in Fig. 11 ($T_c = 2.475$ K). The temperature dependence of H_{c2} is linear as expected from the Ginzburg–Landau theory: $dH_{c2,\perp}/dT = 1.6$ kG K^{-1} and $dH_{c2,\parallel}/dT = 17.2$ kG K^{-1}, the anisotropy of H_{c2} near $T_c = 2.475$ K being 8.75 (Fig. 12). The anisotropy

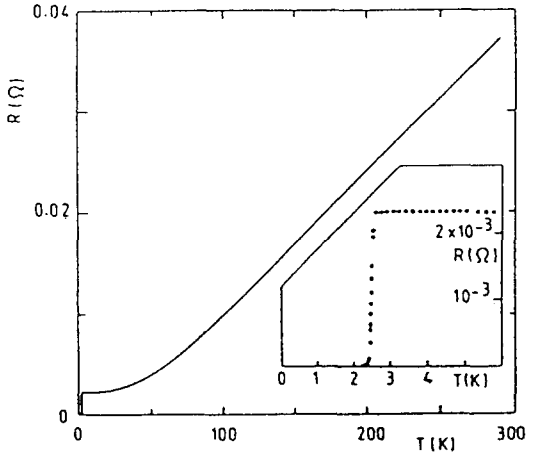

Fig. 11. Temperature variation of the resistance in the (a,b) plane of crystalline $(PbS)_{1.14}NbS_2$. The inset shows the superconducting transition.

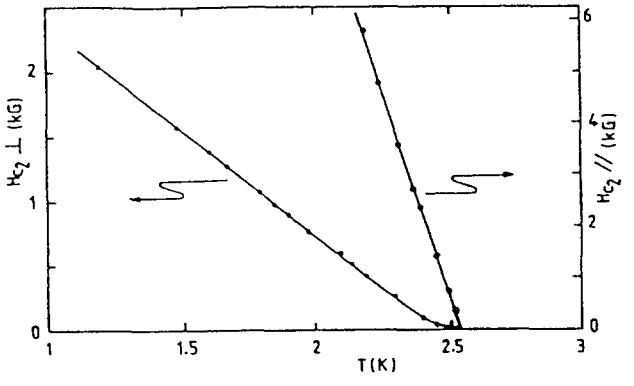

Fig. 12. Temperature variation of H_{c2} of $(PbS)_{1.14}NbS_2$ as a function of temperature when the magnetic field is perpendicular or parallel to the layers.

was also determined from the dependence of H_{c2} on the angle θ between H and the (a,b) plane following $H_{c2}(\theta)/H_{c2,\perp} = \epsilon/(\epsilon^2 \sin^2\theta + \cos^2\theta)^{1/2}$ with $\epsilon = H_{c2,\parallel}/H_{c2,\perp} = (m_\perp/m_\parallel)^{1/2} = 8.97$; $m_\perp$ and $m_\parallel$ are the effective masses. For 2H-NbS_2, $T_c = 6.3$ K, $dH_{c2,\perp}/dT = 7.8$ kG K^{-1} and $dH_{c2,\parallel}/dT = 22.3$ kG K^{-1}, and thus an anisotropy ϵ of 2.9–3.0 is obtained. The first effect of the inclusion of a double PbS layer is to decrease T_c, which can be understood as arising from a proximity effect between the superconducting NbS_2 layers and the insulating PbS layers which weakens the order parameter of the NbS_2 layers. The field dependence of the critical temperature of $(SnS)_{1.17}NbS_2$ and $(PbS)_{1.13}TaS_2$ has been measured [49,50]. The anisotropy factor is ten, about the same as found for $(PbS)_{1.14}NbS_2$ [48].

Specific heat measurements were performed on crystals designated as stoichiometric "MTS_3" [26]. It was concluded [49,50] that the compounds, except $(BiS)_{1.08}TaS_2$, are anisotropic 3D BCS superconductors with a ratio $\Delta C/\gamma T$ ($\Delta C = \gamma T + \beta T^3$) of about 1.2, close to the BCS value of 1.43. From a fit of the H_{c2} data to the usual formula for anisotropic 3D conductors, it was possible to deduce the zero temperature coherence lengths at 0 K, e.g. 290 and 27 Å for $\zeta_\perp(0)$ and $\zeta_\parallel(0)$ respectively of $(SnS)_{1.17}NbS_2$.

$(BiS)_{1.08}TaS_2$ shows a transition from bulk superconductivity below 0.75 K to 1D superconductivity in the temperature range 0.75–1.05 K. Differential resistance measurements of $(BiS)_{1.08}TaS_2$ weak link junctions indicate the presence of superconducting fluctuations up to temperatures as high as 2.4 K, three times the bulk transition temperature of 0.75 K. Experimental observations are in favour of a transition from bulk ($T < 0.75$ K) to 1D (0.75 K $< T_c <$ 1.05 K) superconductivity [50]. Specific heat fluctuations are also present. Furthermore, the ratio $\Delta C/\gamma T$ (=0.6) is much lower than expected for pure BCS behaviour [96].

The compound $(PbS)_{1.14}(NbS_2)_2$ [97] does not show superconductivity down to 1.2 K, which seems to be consistent with the model mentioned above. This may be explained by the 3R stacking type of the two NbS_2 sandwiches (see Fig. 13); indeed, the 3R-NbS_2 polytype is not superconducting in contrast with 2H-NbS_2. The compounds $(PbSe)_{1.12}(NbSe_2)_2$ [98], $(PbSe)_{1.14}(NbSe_2)_2$ [94] (probably identical) and $(LaSe)_{1.14}(NbSe_2)_2$ [95] become superconducting at 3, 3.4 and 5.3 K respectively; the stacking of the paired sandwiches $NbSe_2$ is the same as in 2H-$NbSe_2$ with $T_c = 7.2$ K.

Superconductivity was reported for $(LaS)_{1.14}NbS_2$ ($T_c = 2.43$ K) [8]. Layers of superconducting dichalcogenides present as intercalated defect domains in some misfit compounds may be partly responsible for certain observed properties [33,84].

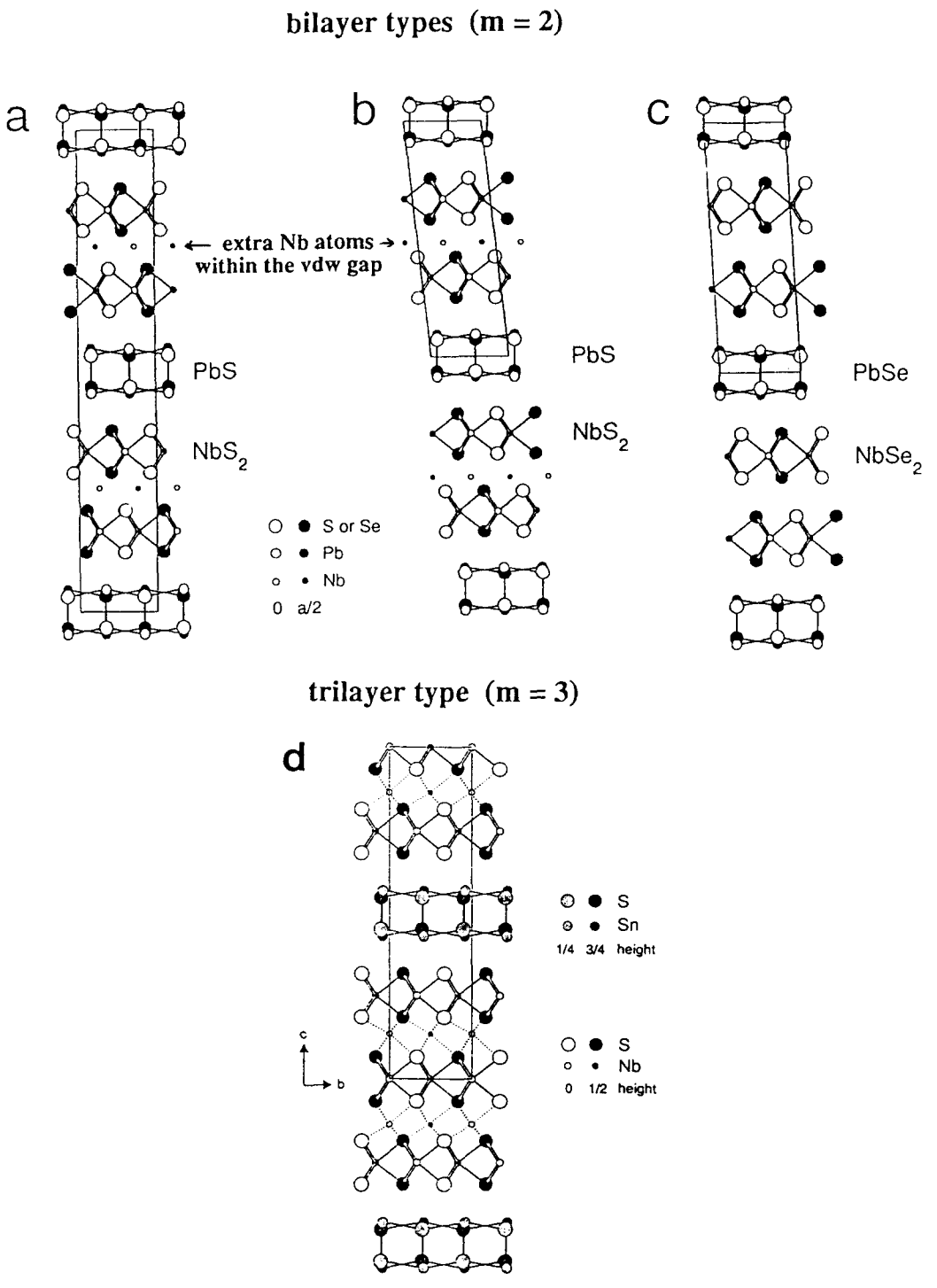

Fig. 13. The projection of (a) "$PbNb_2S_5$" orthorhombic, (b) "$PbNb_2S_5$" monoclinic, (c) "$PbNb_2Se_5$" and (d) "$SnNb_3S_7$" down the $\vec{a}$.

4. Conclusions: discussion of the bonds

Misfit layer chalcogenides represent a very unique series of compounds. They illustrate a case of planar segregation in highly covalent systems. They can also be regarded as "chemical superlattices". The misfit between successive MX and TX_2 slabs is reminiscent of the situation encountered in multilayer systems (e.g. Gd/Y, Fe/Cr,...) usually grown by epitaxial methods.

Meerschaut and coworkers were the first to char-

acterize completely compounds with paired sandwiches ($m = 2$) or tripled sandwiches ($m = 3$) separated by a van der Waals' gap, e.g. $(PbS)_{1.14}(NbS_2)_2$ [97], $(PbS)_{1.18}(TiS_2)_2$ [99], $(PbSe)_{1.12}(NbSe_2)_2$ [98], $(LaSe)_{1.14}(NbSe_2)_2$ [100] and $(SnS)_{1.16}(NbS_2)_3$ [101]; these paired or tripled sandwiches occur as single subsystems (see Fig. 13). Because of the presence of a van der Waals' gap, intercalation by alkali metal atoms [102] or molecules with electron-donating properties [103] seems possible; this has indeed proved to be the case.

When multilayer misfit compounds in a series such as $(LaSe)_{1+x}(NbSe_2)_m$ are prepared, the structure of pure $NbSe_2$ is progressively rebuilt between two LaSe slabs. The good quality of the crystals obtained allows the influence on the properties of the stacking of $[NbSe_2]$ superconducting slabs on top of one another to be evaluated, which is a similar situation to that found in high T_c superconductors.

We have seen the complexity of the magnetic properties which may invoke, at the same time, low dimensionality effects and a modulation of the interactions in an incommensurate structure [104].

Misfit layer compounds show most of the features of low-dimensional chalcogenides: polytypism, intercalation, non- stoichiometry, possibility of exfoliation, etc.

Understanding the nature of the chemical bonds in the misfit layer compounds is not easy. An approach can be made through a critical discussion of the physical properties with respect to the structural type. Also the types of preparation that have been successful, as well as those which have failed, will help us to understand the stability of the structural framework.

The TX_2 slabs that have been observed in misfit compounds are restricted to T elements such as Ti, V, Cr, Nb and Ta, i.e. elements of the left-hand part of the Periodic Table. A phase such as "$LnFeS_3$" [73] has a totally different structural type which can be referred to the structural archetype $Ce_6Al_{10/3}S_{14}$ [105]. This is due to the stability of the TX_2 layered arrangement. Let us come back to the layered dichalcogenides themselves. The band structure scheme shows a valence band essentially built up from anionic s and p orbitals. The corresponding cationic levels have been pushed to higher energies. In between, the d levels of the cation, that have been split by the crystal field, play an essential role with regard to the physical properties according to their degree of filling, energy position, band width, etc. The octahedral slabs result in the classical t_{2g}–e_g splitting, whereas the trigonal prismatic slabs lead to a_1' (mostly d_{z^2} of the metal) below e′ ($d_{xy} + d_{x^2-y^2}$) and e″ (d_{xz},d_{yz}). However, on going to the right of the Periodic Table, the d levels have a progressively lower energy than on the left side and sometimes overlap the sp band. Empty d levels may be filled at the expense of the sp band at the top of which holes will appear. This process is essentially a reduction of the cation (Cr^{3+} and even Fe^{2+} are only stable in the presence of sulphur). In addition, because the top of such an sp band has antibonding character, the anions are now positioned closer to each other, leading at the limit to the formation of anionic pairs such as in pyrite or marcasite.

The instability of Cr^{4+} in the presence of sulphur excludes the existence of a layered chromium disulphide with a stacking of CrS_2 slabs. However, such slabs are found in $NaCrS_2$ where they are separated by Na^+ layers. This is also observed in misfit compounds where CrS_2 slabs are interstacked with LnS slabs. In both cases, chromium has been reduced to Cr^{3+} ions; however, because of the electron transfer from the sodium layer or from the GdS slab to, for example, the CrS_2 slab, the sp band remains full thereby preventing the formation of anionic pairs. The electron transfer seems necessary to stabilize the CrS_2 layers. This hypothesis is also supported by two observations: (a) we could not make misfit phases "$MCrS_3$" with M ≡ Pb and Sn, for which the electron transfer would be very low or zero; (b) we could not make multilayer misfit phases of the type $(LnS)_n(CrS_2)_m$ with $m = 2$, 3 for which the electron transfer would be shared between two or more CrS_2 layers.

The stability can be easily understood in the case of the rare earth derivatives $(LnX)_{1+x}TX_2$. About one electron per rare earth is transferred to the TX_2 slab. In addition to the fact that this will be enough to ensure the stability of unusual TX_2 slabs, such as CrS_2, it leads to the representation of the misfit layer compounds as infinite 2D intercalation compounds. The $(LnS)_{1+x}CrS_2$ phases can be described in this way too, as can $NaCrS_2$, which is similar to $NaTiS_2$, although there is no layered CrS_2.

With M ≡ Pb and Sn, misfit compounds have been obtained only when the TX_2 slabs are stable by themselves. This does not mean that there is no electron transfer at all. It is just that this transfer is not important enough to ensure the stability of a CrS_2 slab, for example. In the case of $(SnS)_{1.17}NbS_2$, an increased occupation of the Nb $4d_{z^2}$ band (a_1' band) was observed [37], indicating charge transfer from the SnS to the NbS_2 subsystem. A recent study associating band structure calculations and photoelectron spectra and comparing $(SnS)_{1.17}NbS_2$, SnS and 2H-NbS_2 has led to the conclusion that there is a transfer of about 0.4 e^- per Nb atom from the SnS to the NbS_2 subsystem [53]. In addition, the band structure calculations show that there is covalent bonding between the two subsystems. Interlayer bonding is particularly strong in the case of $(LaS)_{1.14}NbS_2$.

Finally, it is worth noting that many minerals show misfit layer structures [1,2]. These associate, e.g.

hydroxide-chloride layers in koenenite, sulphide-hydroxide in valleriite and two sulphide layers in cylindrite. The latter shows pseudo-tetragonal MS layers (e.g. PbS) alternating with $M'S_2$ layers (e.g. SnS_2). The geometrical features associated with cylindrite are very similar to those described here for "artificial" misfit compounds. In fact, the minerals have complicated formulations due to solid solutions in each slab and exchanges from one slab to the other. Cylindrite appears as $Pb_{14.3}Sn^{2+}_{5.7}Sb_{4.4}Fe_{1.6}S_{26}$ for the MS slab and $Sn^{4+}_{8.2}Sb_{2.3}Fe_{1.5}S_{24}$ for the $M'S_2$ slab [1]. Both sublattices appear to show modulations (parallel to the misfit direction) and the whole structure can be regarded as the stacking of corrugated sheets. This corresponds to a segregation of cations in rows parallel to $\vec{b}$ depending on their size and according to a minimization of interfacial energies. In addition, the exchange of cations from slab to slab leads to an MS slab that is positively charged and an $M'S_2$ slab that is negatively charged. This may explain the overall stability of the structure, the undulations fixing the position of one slab with respect to the other. Further studies are in progress to determine whether this model may apply, even partially, to the misfit layer compounds described in this paper.

References

[1] E. Makovicky and B.G. Hyde, *Structure Bonding (Berlin), 46* (1981) 101.

[2] A. Meerschaut (ed.), Incommensurate Sandwiched Layered Compounds, *Mater. Sci. Forum,* Trans. Tech. Publ., Vol. 100–101, 1992.

[3] J.S. Anderson, *J. Chem. Soc., Dalton Trans.*, (1973) 1107. I.E. Grey, *J. Solid State Chem., 11* (1974) 128. I.E. Grey, *Acta Crystallogr. Sect. B, 31* (1975) 45. J.T. Hoggins and H. Steinfink, *Acta Crystallogr. Sect. B, 33* (1977) 673. M. Onoda and K. Kato, *Acta Crystallogr. Sect. B, 47* (1991) 630.

[4] M. Saeki and M. Onoda, *J. Solid. State Chem., 102* (1993) 100. M. Onoda, M. Saeki, A. Yamamoto and K. Kato, *Acta Crystallogr. Sect. B, 49* (6) (1993) 929.

[5] R. Brouwer and F. Jellinek, *J. Phys. Coll., 38* (7) (1977) 36. R. Brouwer, Thesis, University of Groningen, Netherlands, 1978.

[6] For a review article, see G.A. Wiegers and A. Meerschaut, in A. Meerschaut (ed.), *Mater. Sci. Forum,* Trans. Tech. Publ., 100–101 (1988) 101.

[7] A. Lafond, A. Sulpice, C. Deudon and A. Meerschaut, *Eur. J. Solid State Inorg. Chem., 31* (1994) 967.

[8] J. Wulff, A. Meetsma, R.J. Haange, J.L. de Boer and G.A. Wiegers, *Synth. Met., 39* (1990) 1.

[9] G.A. Wiegers, A. Meetsma, R.J. Haange and J.L. de Boer, *Mater. Res. Bull., 23* (1988) 1551. S. van Smaalen, *J. Phys.: Condensed Matter, 1* (1989) 2791.

[10] A. Meerschaut, P. Rabu, J. Rouxel, P. Monceau and A. Smontara, *Mater. Res. Bull., 25* (1990) 855–861. G.A. Wiegers, A. Meetsma, R.J. Haange, S. van Smaalen, J.L. de Boer, A. Meerschaut, P. Rabu and J. Rouxel, *Acta Crystallogr. Sect. B, 46* (1990) 324–342.

[11] S. van Smaalen, A. Meetsma, G.A. Wiegers and J.L. de Boer, *Acta Crystallogr. Sect. B, 47* (3) (1991) 314–330.

[12] Y. Ren, A. Meetsma, V. Petricek, S. van Smaalen and G.A. Wiegers, *Acta Crystallogr.*, accepted for publication.

[13] P. Rabu, A. Meerschaut, J. Rouxel and G. Wiegers, *J. Solid State Chem., 88* (1990) 451.

[14] G.A. Wiegers, A. Meetsma, R.J. Haange and J.L. de Boer, *J. Alloys Comp., 178* (1992) 369.

[15] M. Onoda, K. Kato, Y. Gotoh and Y. Oosawa, *Acta Crystallogr. Sect. B, 46* (1990) 487.

[16] K. Kato, I. Kawada and T. Takahashi, *Acta Crystallogr. Sect B, 33* (1977) 3437.

[17] G.A. Wiegers, A. Meetsma, J.L. de Boer, S. van Smaalen and R.J. Haange, *J. Phys.: Condensed Matter, 3* (1991) 2603.

[18] A. Janner and T. Janssen, *Acta Crystallogr. Sect. A, 36* (1980) 408.

[19] For detailed explanations about the method, see S. van Smaalen, *Mater. Sci. Forum, Trans Tech. Publ., 100–101* (1992) 173. S. van Smaalen, *J. Phys. Condensed Matter, 1* (1988) 2789. S. van Smaalen, *Phys. Rev. B, 43* (1991) 11 330.

[20] A. Yamamoto, *Acta Crystallogr. Sect. A, 48* (1992) 476.

[21] K. Kato and M. Onoda, *Acta Crystallogr. Sect. A, 47* (1991) 55. K. Kato and M. Onoda, *Acta Crystallogr. Sect. A, 47* (1991) 448.

[22] K. Kato, *Acta Crystallogr. Sect. B, 46* (1990) 39.

[23] V. Petricek, K. Maly, P. Coppens, X. Bu, I. Ciserova and A. Frost Jensen, *Acta Crystallogr. Sect. A, 47* (1991) 210.

[24] A. Yamamoto, *Acta Crystallogr. Sect. A, 38* (1982) 87.

[25] S. van Smaalen, *J. Phys.: Condensed Matter, 3* (1991) 1247.

[26] P.C. Donohue, *J. Solid State Chem., 12* (1975) 80.

[27] M.H. van Maaren, *Phys. Lett. A, 40* (1972) 353.

[28] L. Schmidt, *Phys. Lett. A, 31* (1970) 551.

[29] L. Schmidt, S.L. McCarthy and J.P. Maita, *Solid State Commun., 8* (1970) 1513.

[30] For a review, see, for example, R.H. Friend and A.D. Yoffe, *Adv. Phys., 36* (1987) 1. J. Rouxel, in F.A. Levy (ed.), *Physics and Chemistry of Layered Materials*, Vol. VI, Reidel, 1979, p. 237. M.S. Whittingham, *Prog. Solid State Chem., 12* (1978) 41. W. Müller-Warmuth and R. Schöllhorm, *Progress in Intercalation Research*, Kluwer, 1994.

[31] C. Sourisseau, R. Cavagnat and J.L. Tirado, *J. Raman Spectrosc., 23* (1992) 647.

[32] M. Hangyo, S. Nakashima, Y. Hamada, T. Nishio and Y. Ohno, *Phys. Rev. B, 48* (15) (1993) 11 291. M. Hangyo, T. Nishio, S. Nakashima, Y. Ohno, T. Terashima and M. Kojima, *J. Appl. Phys., 32* (Suppl. 32–31) (1993) 581.

[33] T. Terashima, N. Kojima, H. Kitagawa, H. Okamoto and T. Mitani, *J. Phys. Soc. Jpn., 62* (6) (1993) 2166.

[34] C.H. Rüscher, C. Haas, S. van Smaalen and G.A. Wiegers, *J. Phys.: Condensed Matter, 6* (1994) 2117.

[35] K. Suzuki, T. Kondo, T. Enoki and H. Tajima, *Mol. Cryst. Liq. Cryst., 245* (1994) 43.

[36] R. Roesky, P. Gressier, A. Meerschaut, K. Widder, H.P. Geserich and G. Scheiber, *J. Phys.: Condensed Matter, 6* (1994) 3427.

[37] Y. Ohno, *J. Phys.: Condensed Matter., 6* (1994) 8655.

[38] A.R.H.F. Ettema, G.A. Wiegers, C. Haas and T.S. Turner, *Phys. Scr., T41* (1992) 265.

[39] A.R.H.F. Ettema, C. Haas and T.S. Turner, *Phys. Rev. B, 47* (1993) 12 794.

[40] A.R.H.F. Ettema and C. Haas, *J. Phys.: Condensed Matter, 5* (1993) 3817.

[41] A.R.H.F. Ettema, S. van Smaalen, C. Haas and T.S. Turner, *Phys. Rev. B, 49* (15) (1994) 10585.

[42] Y. Ohno, *Phys. Rev. B, 48* (8) (1993) 5515.

[43] Y. Ohno, *J. Phys.: Condensed Matter, 4* (1992) 7815.

[44] Y. Ohno, *Phys. Rev. B, 44* (3) (1991) 1281.

[45] K. Suzuki, T. Enoki and S. Bandow, *Phys. Rev. B, 48* (1993) 11 077.

[46] T. Terashima and N. Kojima, *J. Phys. Soc. Jpn., 63* (2) (1994) 658.
[47] C.M. Fang, J. Baas and G.A. Wiegers, to be published.
[48] A. Smontara, P. Monceau, L. Guémas, A. Meerschaut, P. Rabu and J. Rouxel, *Fizika, 21* (1989) 201.
[49] D. Reefman, J. Baak, H.B. Brom and G.A. Wiegers, *Solid State Commun., 75* (1990) 47.
[50] D. Reefman, P. Koorevaar, H.B. Brom and G.A. Wiegers, *Synth. Met., 41–43* (1991) 3775.
[51] H.J.M. Bouwmeester, A. van der Lee, S. van Smaalen and G.A. Wiegers, *Phys. Rev. B, 43* (1991) 9431.
[52] A. Diedering, R.J. Haange and G.A. Wiegers, to be published.
[53] C.M. Fang, A.R.H.F. Ettema, C. Haas, G.A. Wiegers, H. van Leuken and R.A. de Groot, *Phys. Rev. B*, submitted for publication.
[54] K. Suzuki, T. Kondo, T. Enoki and S. Bandow, *Synth. Met., 56* (1993) 1741.
[55] G.A. Wiegers, A. Meetsma, R.J. Haange and J.L. de Boer, *J. Less-Common Met., 68* (1991) 347.
[56] S. van Smaalen and V. Petricek, *Acta Crystallogr. Sect. A, 48* (1992) 610.
[57] G.A. Wiegers and R.J. Haange, *Eur. J. Solid State Inorg. Chem., 28* (1991) 1071.
[58] C. Auriel, A. Meerschaut, C. Deudon, J. Baas, G.A. Wiegers, P. Monceau and C. Chen, to be published.
[59] M. Inoue, M. Koyano, H. Negishi, Y. Ueda and H. Sato, *Phys. Status Solidi B, 132* (1985) 295.
[60] P.C. Klipstein, A. Bagnall, W.Y. Liang, E.A. Marseglia and R.H. Friend, *J. Phys. C: Solid State Phys., 14* (1981) 4667.
[61] P.C. Klipstein and R.H. Friend, *J. Phys. C: Solid State Phys., 20* (1987) 4169.
[62] J.I. Meakin, P.C. Klipstein and R.H. Friend, *J. Phys. C.: Solid State Phys., 00* (1981) L789.
[63] Y. Moelo, A. Meerschaut, C. Auriel and J. Rouxel, *Chem. Mater.*, in press.
[64] D.W. Murphy, C. Cross, F.J. DiSalvo and J.W. Waszczak, *Inorg. Chem., 16* (1977) 3027.
[65] B. van Laar and D.J.W. Ijdo, *J. Solid State Chem., 3* (1971) 590.
[66] G.A. Wiegers, R. van der Meer, H. van Heiningen, H.J. Kloosterboer and A.J.A. Alberink, *Mater. Res. Bull., 9* (1974) 1266.
[67] C.F. van Bruggen, C. Haas and G.A. Wiegers, *J. Solid State Chem., 27* (1979) 9.
[68] T. Kondo, K. Suzuki and T. Enoki, *Solid State Commun., 84* (1992) 999.
[69] K. Suzuki, T. Kondo, T. Enoki and S. Bandow, *Synth. Met., 56* (1993) 1741.
[70] N. Cho, S. Kikkawa, F. Kanamura, Y. Takeda, O. Yamamoto, H. Kido and T. Hoshikawa, *Solid State Ionics, 63–65* (1993) 696.
[71] J. Baas, A. Meetsma and G.A. Wiegers, to be published.
[72] T. Takahashi, S. Osaka and O. Yamada, *J. Phys. Chem. Solids, 43* (1973) 1131.
[73] T. Murugesan, S. Ramesh, J. Gopalakrishnan and C.N.R. Rao, *J. Solid State Chem., 38* (1981) 165.
[74] J. Rouxel, Y. Moëlo, A. Lafond, F.J. DiSalvo, A. Meerschaut and R. Roesky, *Inorg. Chem., 33* (1994) 3358.
[75] Y. Ren, J. Baas, A. Meetsma, J.L. de Boer and G.A. Wiegers, to be published.
[76] J. Rigoult, C. Guidi-Morosini, A. Thomas and P. Molinié, *Acta Crystallogr. Sect. B, 38* (1982) 1557.
[77] D.W. Murphy, F.J. DiSalvo, G.W. Hull and J.V. Waszczak, *Inorg. Chem., 15* (1976) 17.
[78] J.R. Bloembergen, R.J. Haange and G.A. Wiegers, *Mater. Res. Bull., 12* (1977) 1103.
[79] G.A. Wiegers and R.J. Haange, *J. Phys.: Condensed Matter, 2* (1990) 445.
[80] O. Pena, A. Meerschaut and P. Rabu, *J. Magn. Magn. Mater., 104–107* (1992) 1249. O. Pena, P. Rabu and A. Meerschaut, *J. Phys.: Condensed Matter., 3* (1991) 9929.
[81] T. Terashima, N. Kojima, K. Suzuki and T. Enoki, *Solid State Commun., 84* (10) (1992) 963.
[82] T. Terashima and N. Kojima, *J. Phys. Soc. Jpn., 61* (9) (1992) 3303.
[83] K. Suzuki, T. Enoki and K. Imeada, *Solid State Commun., 78* (1991) 73.
[84] K. Suzuki, N. Kojima, T. Ban and K. Tsujikawa, *J. Phys. Soc. Jpn., 59* (1990) 266.
[85] K. Suzuki and T. Enoki, *Mater. Sci. Forum, 91–93* (1992) 369.
[86] A. Lafond, P. Molinié, A. Sulpice, J.L. Tholence, A. Meerschaut and P. Monceau, *C.R. Acad. Sci. Paris, 315* (Série II) (1992) 1673.
[87] K. Suzuki, T. Kondo, M. Iwasaki and T. Enoki, *Jpn. J. Appl. Phys., 32* (Suppl. 32-3) (1993) 341.
[88] R. Roesky, A. Meerschaut, P. Gressier and J. Rouxel, *Mater. Res. Bull., 29* (9) (1994) 943.
[89] F.M.R. Engelsman, B. van Laar, G.A. Wiegers and F. Jellinek, *J. Solid State Chem., 6* (1973) 574.
[90] P.F. Bongers, C.F. van Bruggen, J. Koopstra, W.P.F.A.M. Omloo, G.A. Wiegers and F. Jellinek, *J. Phys. Chem. Solids, 29* (1968) 997.
[91] B. van Laar and F.M.R. Engelsman, *J. Solid State Chem., 6* (1973) 384.
[92] A. Lafond, A. Meerschaut, J. Rouxel, A. Sulpice and J.L. Tholence,, *Phys. Rev. B*, to be submitted.
[93] A. Lafond and A. Meerschaut, *Mater. Res. Bull., 28* (1993) 979.
[94] Y. Oosawa, Y. Gotoh, J. Akimoto, T. Tsunoda, M. Sohma and M. Onoda, *Jpn. J. Appl. Phys., 31* (1992) L1096.
[95] R. Roesky, A. Meerschaut, J. Rouxel and J. Chen, *Z. Anorg. Chem., 619* (1993) 117.
[96] M.A. Hamersma, C.J. Muller, D. Reefman and J.M. van Ruitenbeek, *Physica C, 197* (1992) 106.
[97] A. Meerschaut, L. Guémas, C. Auriel and J. Rouxel, *Eur. J. Solid State Inorg. Chem., 27* (1990) 557.
[98] C. Auriel, A. Meerschaut, R. Roesky and J. Rouxel, *Eur. J. Solid State Inorg. Chem., 29* (1992) 1079.
[99] A. Meerschaut, C. Auriel and J. Rouxel, *J. Alloys Comp., 183* (1992) 129.
[100] R. Roesky, A. Meerschaut, J. Rouxel and J. Chen, *Z. Anorg. Allg. Chem., 619* (1993) 117.
[101] L. Hoistad, A. Meerschaut, P. Bonneau and J. Rouxel, *J. Solid State Chem., 114* (1994) 435.
[102] L. Herman, J. Morales, J. Pattanayak and J.L. Tirado, *J. Solid State Chem., 100* (1992) 262. L. Herman, J. Morales, L. Sanchez and J.L. Tirado, *Solid State Ionics, 58* (1992) 179. C. Barriga, P. Lavela, J. Morales and J.L. Tirado, *Solid State Ionics, 63–65* (1993) 450.
[103] Y. Oosawa, Y. Gotoh, J. Akimoto, M. Sohma, T. Tsunoda and H. Hayakawa, *Solid State Ionics, 67* (1994) 287.
[104] A. Lafond, *Thesis*, University of Nantes, France, 1994.
[105] D. de Saint Giniez, P. Laruelle and J. Flahaut, *C.R. Acad. Sci. Paris, 267* (1968) 1029.
[106] G.A. Wiegers, A. Meetsma, R.J. Haange and J.L. Boer, *Solid State Ionics, 32/33* (1989) 183.
[107] J. Wullf, A. Meetsma, S. van Smaalen, R.J. Haange, J.L. de Boer and G.A. Wiegers, *J. Solid State Chem., 84* (1990) 118.
[108] W.Y. Zhou, A. Meetsma, J.L. de Boer and G.A. Wiegers, *Mater. Res. Bull., 27* (1992) 563.
[109] G.A. Wiegers and R.J. Haange, *J. Phys.: Condensed Matter, 2* (1990) 455.
[110] G.A. Wiegers, A. Meetsma, R.J. Haange and J.L. Boer, *J. Solid State Chem., 89* (1990) 328.